

PUB-77-117-E
E-0034

MEASUREMENTS OF CASCADES INITIATED BY 5-300 GeV HADRONS
IN A TUNGSTEN IONIZATION SPECTROMETER*

L. Cheshire,** R. W. Huggett and W. V. Jones
Department of Physics and Astronomy
Louisiana State University
Baton Rouge, Louisiana (USA) 70803

and

W. K. H. Schmidt*** and M. Simon****
Max Planck Institut für Extraterrestrische Physik
D-8046 Garching bei München, W-Germany

Abstract

The response of a tungsten-scintillator ionization spectrometer to accelerated particle beams has been investigated. Results obtained from exposure of the apparatus to 5, 10, and 15 GeV/c pions as well as to 100, 200, and 300 GeV/c protons are presented. The results include cascade development curves, fractions of the primary energy measured by the spectrometer, and resolutions of the apparatus for measuring the primary energies. The responses of spectrometers having depths smaller than the total depth of $\sim 1000 \text{ g/cm}^2$ were estimated by successively omitting signals from the downstream end of the modular apparatus. The measurements show remarkably good agreement with our Monte Carlo simulations of the cascade development.

1. INTRODUCTION

A tungsten-scintillator ionization spectrometer (calorimeter) has been exposed to 100, 200, and 300 GeV/c protons at the Fermi National Accelerator Laboratory (FNAL). The same apparatus had previously been exposed to 5, 10, and 15 GeV/c pions and electrons at the Stanford Linear Accelerator Center (SLAC) and also to 2.1 GeV/c nucleon ^{12}C and ^{16}O beams at the Lawrence Berkeley Laboratory (LBL). The spectrometer was built as a prototype for a satellite experiment¹ to measure energy spectra and charge composition of high energy cosmic rays.

Results for the fragmentation cross sections of ^{12}C and ^{16}O in CsI and tungsten have been presented previously,² as have measurements on the interaction mean free path of pions in tungsten³ and other data obtained in the exposures at SLAC⁴. Results from the exposures at FNAL are presented here. The data from both SLAC and FNAL are also compared with the results of a Monte Carlo computer program for simulating nuclear-electromagnetic cascades in dense materials.

2. APPARATUS

The apparatus used in the FNAL experiment is shown schematically in Fig. 1. (The experimental configuration is very similar to that used at LBL and at SLAC. Re-

ferences 2-4 contain a more detailed description of the apparatus than is given here.) Wire spark chambers SC_1 and SC_2 provided trajectory information which was used for event selection in analyzing the data. An event trigger was defined by plastic scintillators S_2 and S_3 . Plastic scintillators B_1 and B_2 , each 5 cm in diameter and 0.65 cm thick, were used to tag beam particles passing through the center of the spectrometer. This information was intended to supply some knowledge of the incident particle trajectory in case of a spark chamber failure. However, for much of the data accumulation, this tag was required in the event trigger, in order to obtain as many events as possible with trajectories in the central region of the spectrometer. The results presented here are, unless otherwise indicated, for events satisfying a $B_1 \cdot S_2 \cdot B_2 \cdot S_3$ trigger requirement.

The target consisted of a stack of five CsI(Tl) crystal detectors viewed by separate photomultipliers. Each crystal was 2 cm (9 g/cm^2) thick and was immersed in oil in a plexiglass casing with walls 1 mm thick.

Modules $T_1 - T_5$ are called high resolution modules (we shall refer to these modules, collectively, by the abbreviation HRM). Each consisted of a 13 g/cm^2 thick tungsten layer (95% W, 5% Ni) followed by a 0.65 cm thick sheet of plastic scintillator. Each module was viewed by a separate photomultiplier. Each of the eleven thick

modules $T_6 - T_{16}$ consisted of four layers of tungsten (total thickness 79 g/cm^2) and three sheets of 0.65 cm thick plastic scintillator arranged in alternating layers, with 26.3 g/cm^2 or 3.7 radiation lengths (r.l.) of tungsten between each pair of scintillators. A photomultiplier on each of the two opposite sides of the module viewed all three scintillators. The signals from the two photomultipliers were added electronically, and the resulting signal was used to determine the response of the module. Thus, although the ionization was sampled every 3.7 r.l., the signal from a module was a measure of the average ionization over the entire module (11.1 r.l.).

3. RESULTS

Cascade Curves. Figure 2 shows, for several incident-particle energies, the average number of equivalent particles $\langle n \rangle$ in the cascade as a function of depth t in the spectrometer. By number of equivalent particles, one usually means the total ionization energy loss rate expressed in units of the energy loss rate of some standard particle. Since the ionization energy loss rate of a charged particle is a statistical process, sometimes the peak and sometimes the mean of the standard particle's energy loss distribution is used. We have chosen the mean of the energy loss distribution for vertically-incident

cosmic ray muons to define an equivalent particle.

The 300 GeV/c data were obtained from a beam which was essentially 100% protons, while the 200 GeV/c and 100 GeV/c data were for mixed proton-pion beams. The pion contaminations are estimated to be 5% and 50%, respectively, at 200 GeV/c and 100 GeV/c. The data at 5, 10, and 15 GeV/c were obtained for negative pions at SLAC and have been presented previously in Ref. 4. In Ref. 4 these cascade curves were expressed in units of the average energy loss rate of a 15 GeV/c pion. They are expressed here in terms of the average energy loss of sea-level cosmic ray muons.

The cascade curves shown in Fig. 2 are for events in which the signal from each CsI module was less than two equivalent particles. The curves rise rapidly in the tungsten modules, with the maxima occurring at progressively greater depths in the spectrometer with increasing incident energy. The number of particles in a cascade at the maximum is given approximately by the relation

$$\langle n \rangle_{\max} = 1.3 (E_0)^{0.9} \quad (1)$$

where E_0 is the incident energy in GeV. At depths far beyond the maximum each cascade dies out exponentially.

In Fig. 3, for the 300 GeV/c proton and 15 GeV/c pion data, separate cascade development curves are shown

for all events and for the subset of those events in which the first interaction of the incident particle occurred near the top of the spectrometer (in the HRM). Localizing the first interaction results in two rather striking features: (1) the cascade maximum contains about twice as many particles as does the maximum of the corresponding cascade for all events; and (2) for the 300 GeV/c data, the cascade curve exhibits a significant change in slope just beyond the maximum. The greater average number of particles at the maximum is expected, since the data for all events includes many single particles which have not yet interacted. The explanation for the pronounced peaking in the curve for localized interactions lies in the high inelasticity as well as in the large ratio of the interaction length to the radiation length for tungsten. Cascades curve in lighter materials, such as iron, do not show such pronounced changes in slope.

Energy Measurements. The energy measured in each module of the spectrometer is determined from the number of equivalent particles comprising the cascade in that module. The energy deposited in the scintillator layers of a module is given by the relation

$$\Delta E_{sc} = N_i \cdot t_{sc} \cdot (dE/dx), \quad (2)$$

where N_i is the number of equivalent particles observed

in the scintillator layer(s) of the i^{th} module, t_{sc} is the total thickness of scintillator in that module, and dE/dx is the energy loss rate in scintillator of the equivalent particle. The energy loss in the tungsten layers of the module is then estimated using the relation

$$\Delta E_{\text{w}} = \Delta E_{\text{sc}} R (t_{\text{w}}/t_{\text{sc}}), \quad (3)$$

where t_{w} is the total thickness of tungsten in the module. The factor R includes such effects as different dE/dx rates for electrons in the different materials, multiple coulomb scattering, and transition effects. Values for R were determined in a series of Monte Carlo calculations for the various incident energies and particle types. The energy losses ΔE_{w} and ΔE_{sc} are known in a Monte Carlo calculation, hence Eq. (3) can be solved for R . This value could depend, in principle, on the age of the cascade and other factors. However, the values we have obtained are practically independent of incident energy and particle type, so we have chosen to use the same value, $R = 0.78$, for all calculations involving tungsten and scintillator.

The energy loss in a material other than tungsten is estimated in a similar manner, i.e., by scaling the measured energy loss in the scintillator layers (or other signal-producing elements, e.g., the CsI layers)

by the ratio of relative thicknesses ($t_{\text{mat}}/t_{\text{sc}}$) and by the appropriate factor R . The total energy loss in any module is, of course, equal to the sum of the energy losses in the various materials comprising the module. A sum over all modules then gives the total energy measured by the spectrometer.

Figure 4 shows, for 15 GeV/c pions and for 300 GeV/c protons, the measured energy distributions for spectrometers of several different total depths. The data were all obtained using the same spectrometer, which has a total depth $\sim 1000 \text{ g/cm}^2$. However, by not including in the analysis one or more modules from the downstream end, we effectively obtain a shorter spectrometer. Some particles from interactions in the downstream modules contribute to the signal observed in nearby upstream modules⁵. Excluding the downstream modules from the analysis does not eliminate this "backscattered" contribution. Nevertheless, some idea of the performance of the spectrometer as a function of depth can be obtained.

In Fig. 4 distributions are shown for the measured energy E_m (as a percentage of the total energy E_0 of the incident particle). Each distribution has been normalized to 5000 total events to facilitate comparisons. (There were actually 7376 pion events and 2545 proton events in the data sets.) The "peak" on the left side of the distributions for shallow depths represents particles which have not yet interacted. It may, in the distri-

butions for pions, also include muons from pion decays upstream. As the depth increases, more and more of the incident particles interact, and the "non-interacting" peak consequently decreases. The peak does not appear if the incident particles are required to interact in the HRM or elsewhere near the top of the spectrometer (distributions not shown). In the analysis of the pion data, the muon contamination was removed (or greatly reduced) by requiring a signal of at least five particles in one or more of the tungsten modules. This effectively requires an interaction somewhere in the spectrometer. Pions which penetrated the full depth without interacting were also eliminated, since they are indistinguishable from muons under this criterion.

The broad peak at higher values of E_m/E_0 represents cascades initiated by particles which have interacted. At shallow depths the cascades are in various stages of development, giving rise to a rather broad peak. At greater depths, more fully developed cascades cause the peak to become narrower and the centroid to shift toward higher values of E_m/E_0 .

The average percentage of the primary energy measured by the total depth of the spectrometer varies from about 70% to about 80% for the primary energies studies in this experiment. Values are given in Table 1 for a) all events, and for b) the subset of those events in

which the first interaction of the incident particle occurred in the HRM. The errors shown are statistical only, and are generally small. More significant are the errors due to uncertainties in the quantities in Eqs. (2) and (3) and, particularly, in the numbers of equivalent particles N_i which, in turn, depend critically on the module calibrations. (See Refs. 2-4.) We estimate that the overall error in each total measured energy is less than 5% of the quoted percentage value.

For the three lowest energies shown in the table, approximately the same percentage of the primary energy is measured irregardless of the location of the first interaction. Hence, the total depth of about 1000 g/cm^2 is apparently adequate to contain most of the cascades. However, for the three higher energies, a somewhat greater percentage of the primary energy is measured when the incident particle interacts in the HRM, implying that the full depth is not adequate for complete containment.

In most applications a spectrometer is used to predict the energy E_0 of the incident particle. Therefore, it is important to know the average response as a function of E_0 . In Fig. 5, our results for $\langle E_m \rangle$ are given as a function of E_0 for three different spectrometer depths. These results are well represented by

$$\langle E_m \rangle = cE_0^3 \quad (4)$$

where $\alpha = 0.73$ and $\beta = 0.89, 0.96,$ and 1.01 for $\frac{1}{2}$ depth, $\frac{1}{2}$ depth, and full depth, respectively, for E_0 in GeV.

Energy Resolution. The energy resolution of the apparatus is taken to be the ratio of the standard deviation to mean for the distribution of measured energies, or σ/E_m . The dependence of the energy resolution on the spectrometer depth t is illustrated in Fig. 6 for 300 GeV/c protons. Curves are shown for the following sets of events:

- a) all incident particles;
- b) particles interacting in the HRM;
- c) particles interacting in the HRM with upper limits on the signals from the last two modules ($T_{16} < 50$ particles, $(T_{15}+T_{16}) < 100$ particles).

The energy resolution improves with increasing t for all three curves. The differences in the curves result from the spectrometer not being sufficiently deep to contain all cascades. The resolution, particularly at shallow depths, is much better when the incident particle interacts near the upstream end of the spectrometer (in the HRM). However, even when the cascade originates in the HRM, considerable energy may still escape out the downstream end. The use of criterion c (bottom curve) provides an estimate of the energy resolution for a much deeper spectrometer, since it selects events whose energy is mostly contained. For large depths there is not much difference in the

energy resolutions for the three criteria.

Energy resolutions for 5 and 15 GeV/c pions, and for 100 and 300 GeV/c protons are shown as a function of spectrometer depth t in Fig. 7. In each case the incident particle was required to have interacted in the HRM, but no requirements were imposed on the energy containment. The resolutions for 5 and 15 GeV/c pions reach plateau values, since most of the cascades are contained within the total depth of about 1000 g/cm^2 . However, for the higher primary energies this depth is not sufficient to contain the cascades.

Energy resolutions for each of the particle beams studied are presented in Table 2. Values are given a) for all events and b) for events in which the first interaction occurred in the HRM.

Events in the tails of a measured energy distribution greatly influence the standard deviation and, hence, the energy resolution. In the 300 GeV/c proton distributions in Fig. 4, for instance, the tails extend almost to zero energy even when the full depth of the spectrometer is used. The tail is due to cascades which are only partially contained in the spectrometer, either because the incident particle interacted late or because of statistical fluctuations in the cascade development. Such events can be rejected by imposing limits on the total measured energy. As the limits are made more re-

strictive, a greater number of events in the tails of a distribution are rejected and the standard deviation decreases. For some data sets the inclusion or exclusion of one or two events has a significant effect on the value obtained for the energy resolution. In determining the energy resolution, we have tried to choose limits such that only events clearly not part of the main peak, i.e., those relatively far out in the tails, are excluded.

The dependence of the energy resolution on the incident energy is shown in Fig. 8. Values are given for three different event selection criteria:

- a) HRM interactions;
- b) HRM interaction with cuts on the total measured energy (to reject events in the low-energy tail);
- c) HRM interaction with cuts on the signals from T_{15} and T_{16} (to accept only events with cascades essentially contained in the spectrometer) and with cuts on the total measured energy.

For each criterion, the energy resolution improves with increasing incident energy. For criterion (a), a plateau value of approximately 10% is reached at about 100 GeV. The plateau results from the poorer energy containment with increasing energy. Most of the events with poor energy containment are found in the low-energy tail of the measured energy distribution and are removed by criterion (b). There are some events, however, whose

total measured energy is in the peak of the distribution, yet a significant amount of energy escapes out the end of the spectrometer. These events are eliminated by criterion (c).

The straight line in Fig. 8, represented by the equation

$$\sigma/E_m (\%) = 46.4 E_o^{-0.337} \quad (E_o \text{ in GeV}) \quad (5)$$

has been drawn to fit the data for criterion (c). This power law dependence is not as steep as that ($\sigma/\mu(\%) = 110.5 E^{-0.5}$) observed by Barish, et al.⁶ The discrepancy may be due in part to the different sampling frequencies of the two experiments. Barish's measurements were made with a sampling frequency of 5.6 r.l. (10 cm in an iron calorimeter), whereas ours were made with a sampling frequency of 3.7 r.l. (1.5 cm in tungsten alloy). The fine sampling should be more important for lower energies. In Fig. 9 the results are compared with additional measurements⁷⁻¹⁰ having a sampling frequency more similar to ours.

4. MONTE CARLO CALCULATIONS

One of the reasons for carrying out this experiment was to check a Monte Carlo program used to predict the cascade development at energies above those available at accelerators. Monte Carlo extrapolations are necessary

for experiments using spectrometers at higher cosmic ray energies.

In Fig. 10 our measurements for cascade development curves (100 GeV/c protons) are compared with Monte Carlo calculations, both for all incident particles and for particles interacting in the HRM. In Fig. 11, the comparisons are made for 15 GeV/c pions interacting in the HRM and for 300 GeV/c protons interacting in T_6 (the first thick tungsten module). The cascade curves are given as a function of the distance (in g/cm^2) from the start of the interaction region, i.e., from the beginning of either the HRM or T_6 , respectively, rather than from the upstream end of the spectrometer. There is generally good agreement between calculations and the data, although the Monte Carlo results for 15 GeV/c are somewhat higher than the data points in the vicinity of the cascade maximum.

Distributions of the total measured energy are shown in Fig. 12 for 15 GeV/c pions for the spectrometers of two different depths. Predictions of the Monte Carlo calculations are indicated by dashed lines. The data are indicated by solid lines. Each distribution has been normalized to 5000 total events. (There were actually 7376 real events and 792 Monte Carlo events.)

Monte Carlo predications for the total measured energy (as a percentage of the primary energy) are pre-

sented in Table 3 for 5, 10, and 15 GeV/c pions, and for 100 and 300 GeV/c protons. Values are given for all incident particles and for particles interacting in the HRM (in T_6 for the 300 GeV/c protons). Because of limited computer time, only 300 GeV/c events with interactions in the first thick tungsten module (T_6) were calculated. Comparison of Tables 1 and 3 shows that the data and the Monte Carlo predictions are in reasonably good agreement over the entire range of energies studied. Differences are typically 1 - 3% of the values quoted for the data.

The energy resolution as a function of spectrometer depth t is shown in Fig. 13 for 100 GeV/c protons. Data as well as predictions of the Monte Carlo calculations are given a) for all incident particles and b) for particles interacting in the HRM. The agreement is generally good, particularly for the HRM-interaction events.

Monte Carlo predictions for the full-depth energy resolution are presented in Table 4 for 5, 10, and 15 GeV/c pions, and for 100 and 300 GeV/c protons. Values are given for all incident particles and for particles interacting in the HRM (in T_6 for the 300 GeV/c protons). Comparison of Tables 2 and 4 shows that the Monte Carlo calculations give somewhat better energy resolutions for pions than are obtained from the experimental data.

One reason may be the presence in the particle beams of muons from pion decays upstream of the apparatus. This beam contamination was reduced by requiring a signal of five or more equivalent particles in at least one spectrometer module. The same selection criteria were applied to both real and Monte Carlo events. However, because of statistical fluctuations, some of the muon events may not have been eliminated. In addition, electrons in the beam could give rise to events on the high-energy side of the measured energy distributions. For 100 GeV/c protons, the energy resolutions for the Monte Carlo events and for the real events are in agreement. For 300 GeV/c protons interacting in T_6 , the energy resolution is somewhat better for the real events than for the Monte Carlo events. It should be mentioned, however, that there were only 148 Monte Carlo events, so that here we are probably statistics-limited.

REFERENCES

- * Research supported by the U.S. National Aeronautics and Space Administration Contract Nos. NAS5-11426 and NAS5-20883 and Grant No. NGR 19-001-012, by the U.S. National Science Foundation, and by the German Science Ministry Grant No. WRK-244.
 - ** Present Address: TRW Systems Group, One Space Park, Redondo Beach, California 90278, USA.
 - *** Present Address: Code 661, NASA, Goddard Space Flight Center, Greenbelt, Maryland 20771, USA.
 - **** Present Address: Gesamthochschule, 59 Siegen 21, Fachbereich Physik, Hölderlinstrasse 3, W-Germany.
1. J. F. Ormes, V. K. Balasubrahmanyam, T. Bowen, R. W. Huggett, T. A. Parnell, and K. Pinkau, "Composition and Spectra of High Energy Cosmic Rays - A Proposal for an Orbiting Laboratory for the HEAO," GSFC Report No. X-661-71-1 (unpublished).
 2. D. L. Cheshire, R. W. Huggett, D. P. Johnson, W. V. Jones, S. P. Rountree, S. D. Verma, W. K. H. Schmidt, R. J. Kurz, T. Bowen and E. P. Krider, Phys. Rev. D 10 (1974) 25.
 3. D. L. Cheshire, R. W. Huggett, W. V. Jones, S. P. Rountree, W. K. H. Schmidt, R. J. Kurz, T. Bowen, D. A. DeLise, E. P. Krider, and C. D. Orth, Phys. Rev. D 12 (1975) 2587.

4. D. L. Cheshire, R. W. Huggett, D. P. Johnson, W. V. Jones, S. P. Rountree, W. K. H. Schmidt, R. J. Kurz, T. Bowen, D. A. DeLise, E. P. Krider, and C. D. Orth, Nucl. Instrum. Methods 126 (1975) 253.
5. R. W. Ellsworth, J. Goodman, A. Ito, J. MacFall, F. Siohan, R. E. Streitmatter, S. C. Tonwar, and G. B. Yodh, in Proceedings of the Calorimeter Workshop (Fermi National Accelerator Laboratory, Batavia, Illinois, 1975), p. 201.
6. B. C. Barish, J. F. Bartlett, D. Buchholz, T. Humphrey, F. S. Merritt, Y. Nagashima, F. J. Sciulli, D. Shields, H. Suter, G. Krafczyk, and A. Maschke, Nucl. Instrum. Methods 116 (1974) 413.
7. J. Engler, W. Flauger, B. Gibbard, F. Monnig, K. Runge, and H. Schopper, Nucl. Instrum. Methods 106 (1973) 189.
8. A. Benvenuti, D. Cline, W. T. Ford, R. Imlay, T. Y. Ling, A. K. Mann, F. Messing, J. Pilcher, D. D. Reeder, C. Rubbia, R. Stefanski, and L. Sulak, Nucl. Instrum. Methods 125 (1975) 447.
9. F. Turkot, E. Harvey, T. Kondo, W. Kononenko, E. M. O'Neill, W. Selove, R. Diamond, A. R. Erwin, R. Loveless, and M. Thompson, University of Pennsylvania Internal Report (unpublished) 1973.
10. L. W. Jones, J. P. Chanowski, H. R. Gustafson, M. J. Longo, P. L. Skubic, J. L. Stone, and B. Cork, Nucl. Instrum. Methods 118 (1974) 431.

11. W. V. Jones in Proceedings of the Calorimeter Workshop
(Fermi National Accelerator Laboratory, Batavia,
Illinois, 1975), p. 41.

TABLE 1. Percentage of the primary energy measured by the spectrometer. The indicated errors are statistical only.

<u>Incident Particle</u>	E_m/E_o (%)	
	<u>All Events</u>	<u>HRM Interaction</u>
5 GeV/c π	72.8 \pm 1.2	73.9 \pm 2.1
10 GeV/c π	72.6 \pm 0.7	72.5 \pm 1.1
15 GeV/c π	72.6 \pm 0.2	71.7 \pm 0.4
100 GeV/c p	75.5 \pm 0.3	78.5 \pm 0.3
200 GeV/c p	75.3 \pm 0.4	78.4 \pm 0.3
300 GeV/c p	75.1 \pm 0.3	79.0 \pm 0.3

Table 2. Energy resolution -- the ratio (given as a percentage) of the standard deviation to the mean of the distribution of measured energies. The indicated errors are statistical only.

<u>Incident Particle</u>	σ/E_m (%)	
	<u>All Events</u>	<u>HRM Interaction</u>
5 GeV/c π	32.3 \pm 0.6	27.7 \pm 1.1
10 GeV/c π	27.1 \pm 0.5	21.8 \pm 0.7
15 GeV/c π	22.5 \pm 0.2	18.4 \pm 0.3
100 GeV/c p	12.4 \pm 0.2	9.9 \pm 0.2
200 GeV/c p	11.7 \pm 0.2	8.6 \pm 0.3
300 GeV/c p	11.8 \pm 0.2	7.7 \pm 0.2

TABLE 3. Percentage of the primary energy measured by the spectrometer as predicted by the Monte Carlo results. The indicated errors are statistical only.

Incident Particle	E_m/E_0 (%)	
	All Events	HRM/T ₆ Interaction
5 GeV/c π	70.4 \pm 0.6	69.4 \pm 1.0
10 GeV/c π	71.4 \pm 0.6	71.7 \pm 0.9
15 GeV/c π	73.7 \pm 0.5	73.4 \pm 0.7
100 GeV/c p	75.3 \pm 1.0	76.4 \pm 0.6
300 GeV/c p	-----	78.6 \pm 0.6

TABLE 4. Energy resolution of the spectrometer as predicted by the Monte Carlo results. The indicated errors are statistical only.

<u>Incident Particle</u>	σ/E_m (%)	
	<u>All Events</u>	<u>HRM/T₆ Interaction</u>
5 GeV/c π	28.7 \pm 0.6	23.9 \pm 0.5
10 GeV/c π	22.8 \pm 0.6	20.0 \pm 0.9
15 GeV/c π	18.3 \pm 0.5	13.1 \pm 0.7
100 GeV/c p	12.4 \pm 0.7	9.4 \pm 0.5
300 GeV/c p	-----	9.1 \pm 0.5

FIGURE CAPTIONS

- Fig. 1. Scale drawing of the apparatus. SC_1 and SC_2 are wire spark chambers; B_1 , B_2 , S_1 , S_2 , and S_3 are plastic scintillators.
- Fig. 2. Cascade development curves. Results for: 5 GeV/c pions - \triangle , 10 GeV/c pions - \diamond , 15 GeV/c pions - \circ , 100 GeV/c protons - Δ , 200 GeV/c protons - \square , 300 GeV/c protons - \bigcirc . Statistical errors ($\sigma\sqrt{N}$, where σ is the standard deviation and N is the number of events) are shown when larger than the symbols.
- Fig. 3. Cascade development curves. Results for 15 GeV/c pions: All events - \circ , Interaction in HRM - Δ . Results for 300 GeV/c protons: All events - \bigcirc , Interaction in HRM - Δ . Statistical errors ($\sigma\sqrt{N}$) are indicated when larger than the symbols.
- Fig. 4. Distributions of the total measured energy E_m given as a percentage of the incident energy E_0 , for various spectrometer depths. The numbers of events per one-percent intervals in E_m/E_0 are shown. All distributions have been normalized to 5000 total events.
- Fig. 5. Average measured energy $\langle E_m \rangle$ as a function of the incident energy E_0 . Results for the following spectrometer depths: $\frac{1}{4}$ depth - \triangle , $\frac{1}{2}$ depth - \circ , full depth - \bigcirc .
- Fig. 6. Energy resolution for 300 GeV/c protons as a function of spectrometer depth t . All events: \bigcirc . Interaction in the HRM: Δ . Interaction in the HRM, and

$T_{16} < 50$ particles, $T_{15} + T_{16} < 100$ particles: Δ .

Fig. 7. Energy resolution as a function of spectrometer depth t . Results for: 5 GeV/c pions - Δ , 15 GeV/c pions - \triangle , 100 GeV/c protons - \circ , 300 GeV/c protons - \bigcirc .

Fig. 8. Energy resolution as a function of incident energy E_0 . Results for: (a) HRM interaction - \bigcirc ; (b) HRM interaction, no low-energy tail - \circ ; (c) HRM interaction, cascade contained in spectrometer, no low-energy tail - Δ .

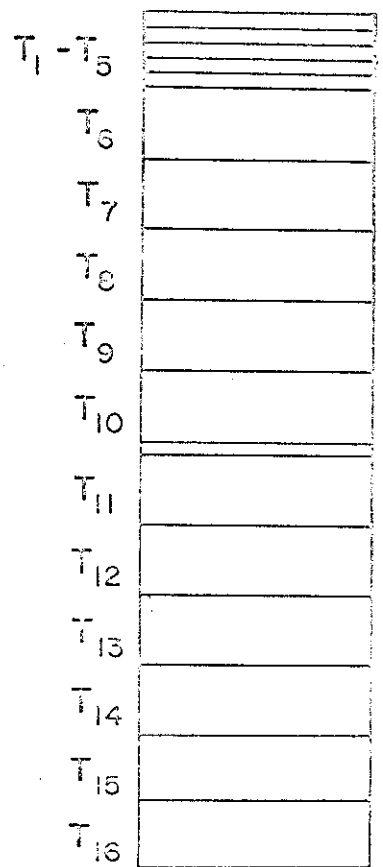
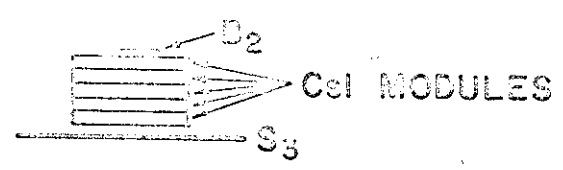
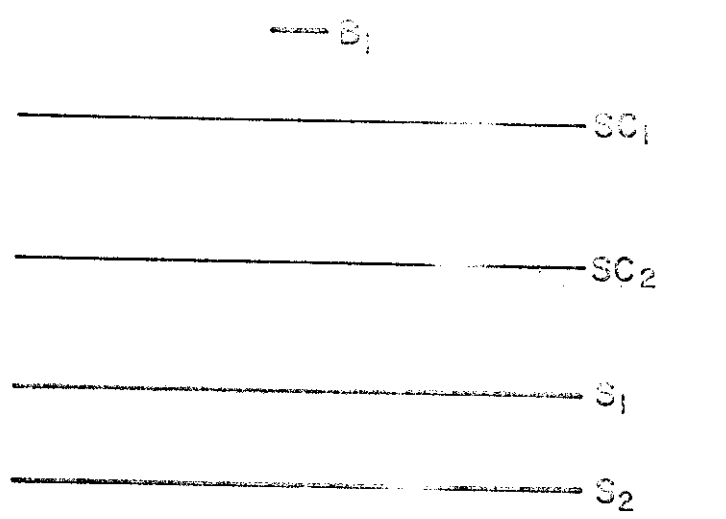
Fig. 9. Energy resolution as a function of incident energy E_0 . Results for: Ref. 6 - \circ , Ref. 7 - Δ , Ref. 8 - \times , Ref. 9 - \square , Ref. 10 - ∇ , this experiment - \bigcirc .

Fig. 10. Cascade development curves for 100 GeV/c protons. Results for all events: data - \circ , Monte Carlo calculations - \bigcirc . Results for events with the first interaction in the HRM: data - Δ , Monte Carlo - Δ . Statistical errors ($\sigma\sqrt{N}$) are shown when larger than the symbols.

Fig. 11. Cascade development curves for a) 15 GeV/c pions which interacted in the HRM: data - Δ , Monte Carlo calculations - Δ ; and b) 300 GeV/c protons which interacted in T_6 : data - \square , Monte Carlo - \bigcirc . Statistical errors ($\sigma\sqrt{N}$) are shown when larger than the symbols.

Fig. 12. Distributions of the total measured energy for 15 GeV/c pions at two different spectrometer depths. Results of Monte Carlo calculations are indicated by dashed lines. The data are indicated by solid lines.

Fig. 13. Energy resolution as a function of spectrometer depth t , for 100 GeV/c protons. Results for all events: data - Δ , Monte Carlo calculations - \triangle . Results for events with first interaction in the HRM: data - \odot , Monte Carlo - \circ .



HIGH RESOLUTION
TUNGSTEN MODULES

THICK TUNGSTEN
MODULES (T₆ - T₁₆)

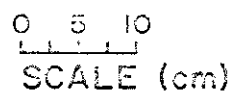


Fig. 1

$\langle n \rangle$ [PARTICLES]

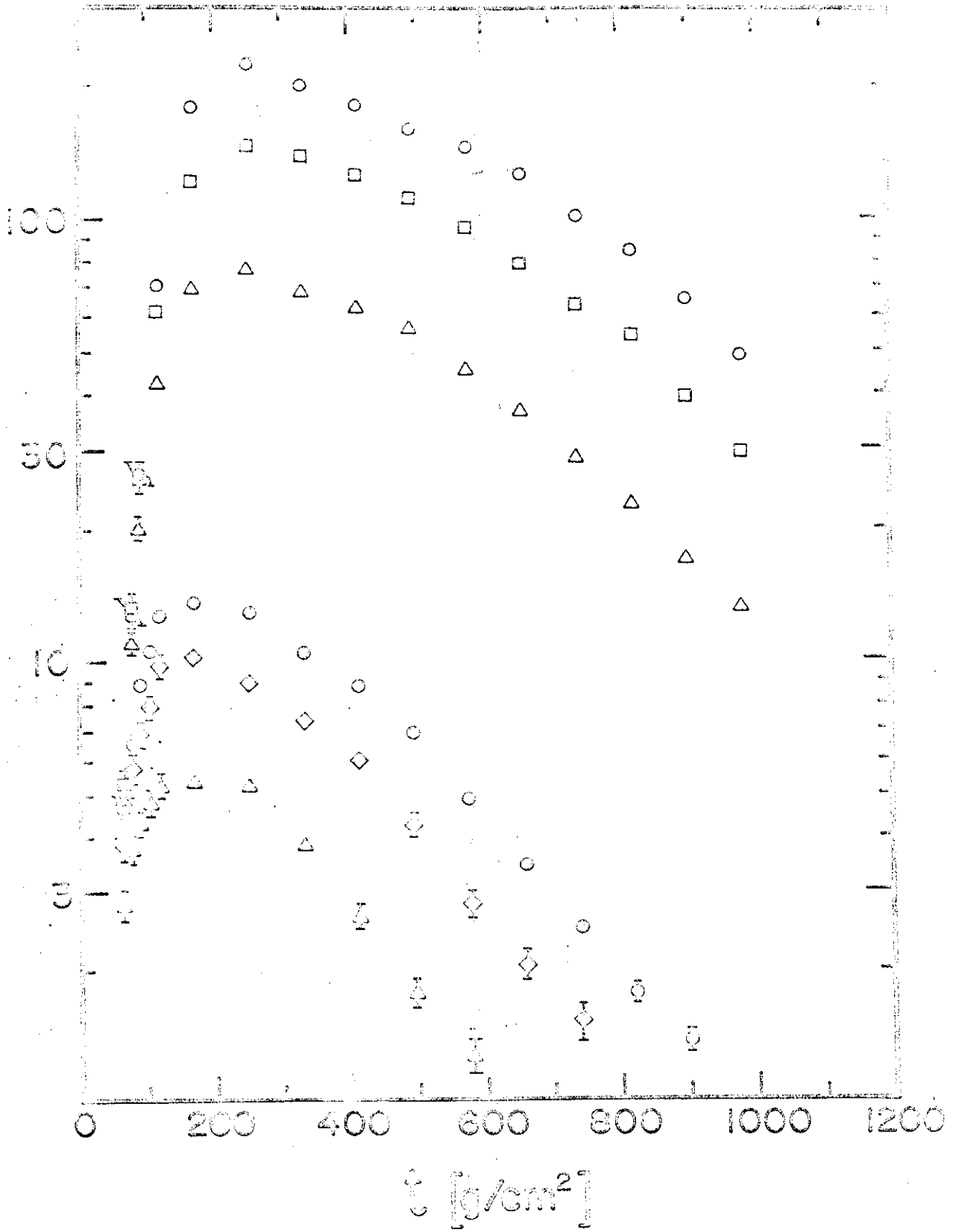


Fig. 2

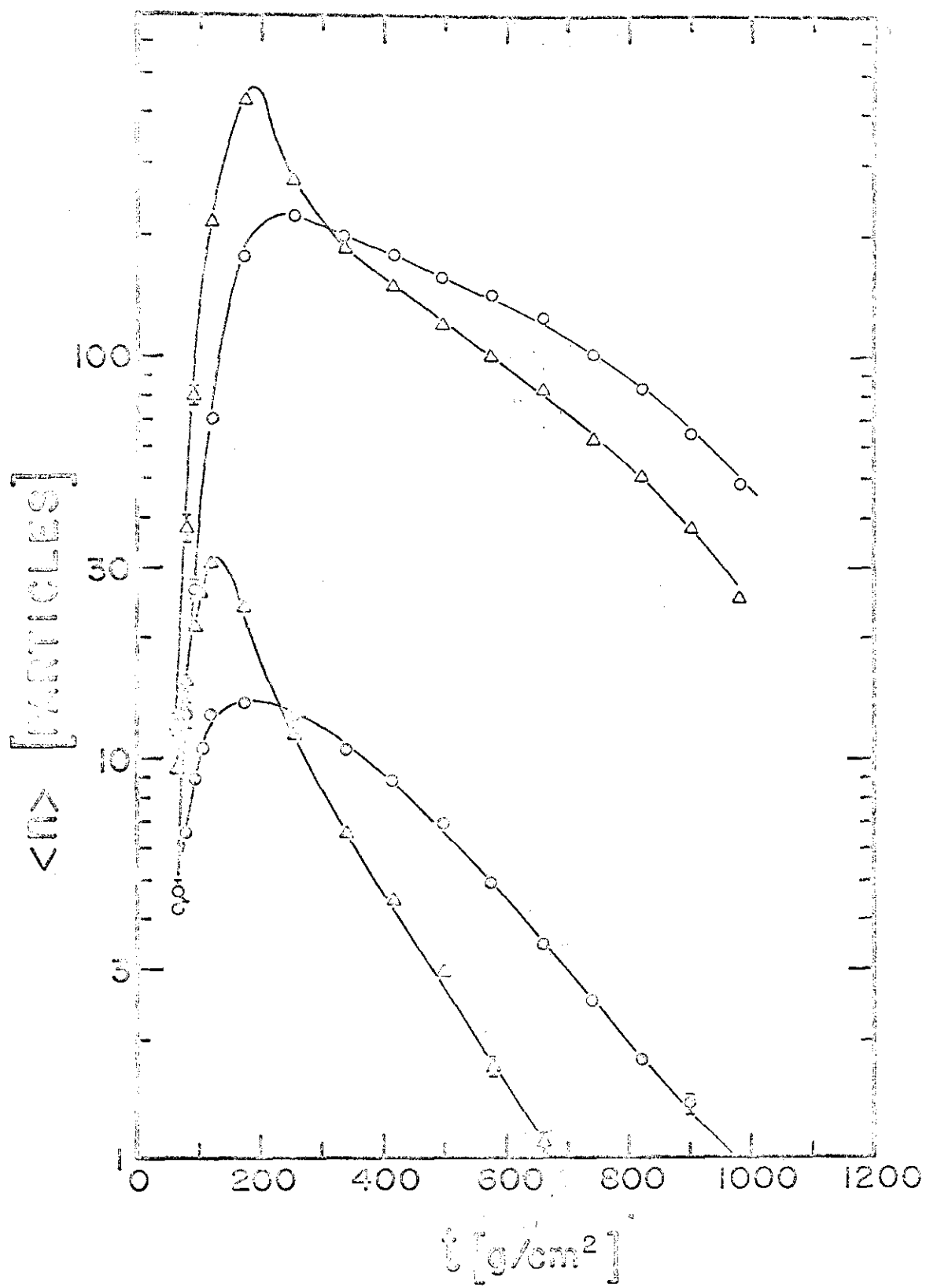
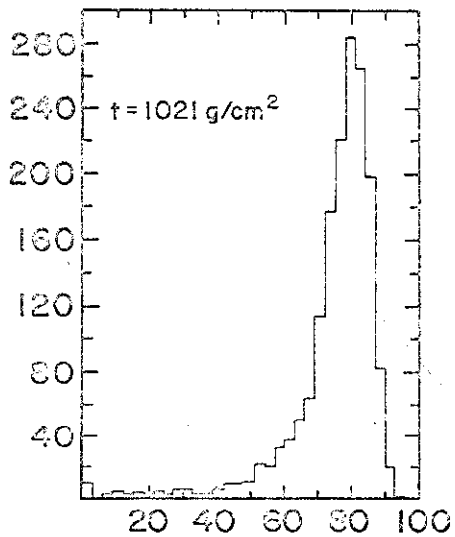
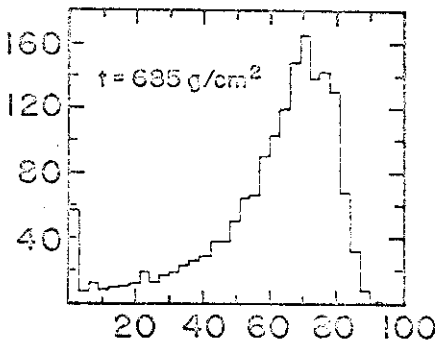
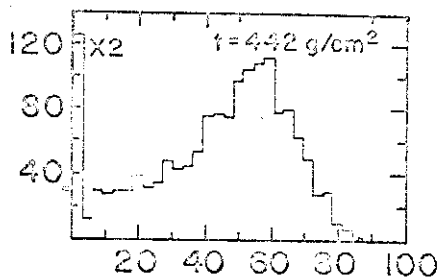
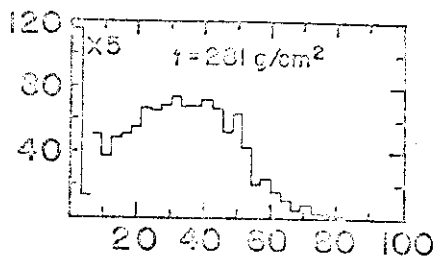
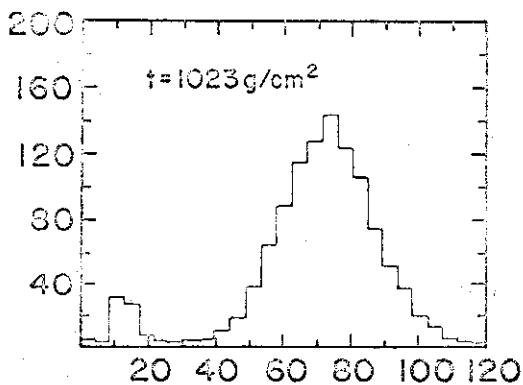
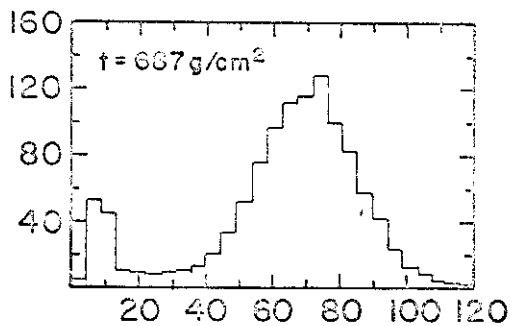
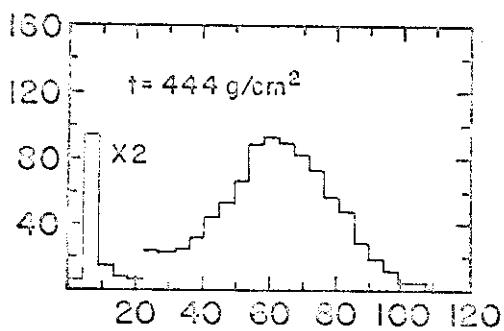
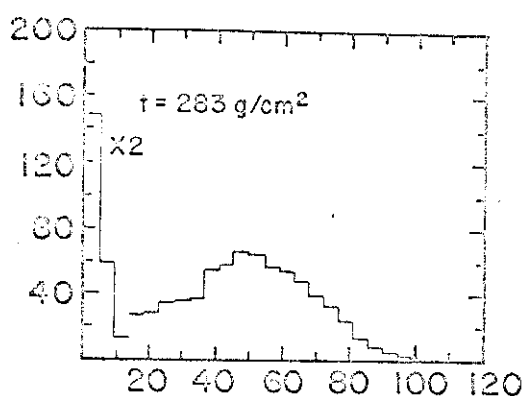


Fig. 3

15 GeV/c PIONS

300 GeV/c PROTONS

NUMBER OF EVENTS



E_m/E_0 [%]

Fig. 4

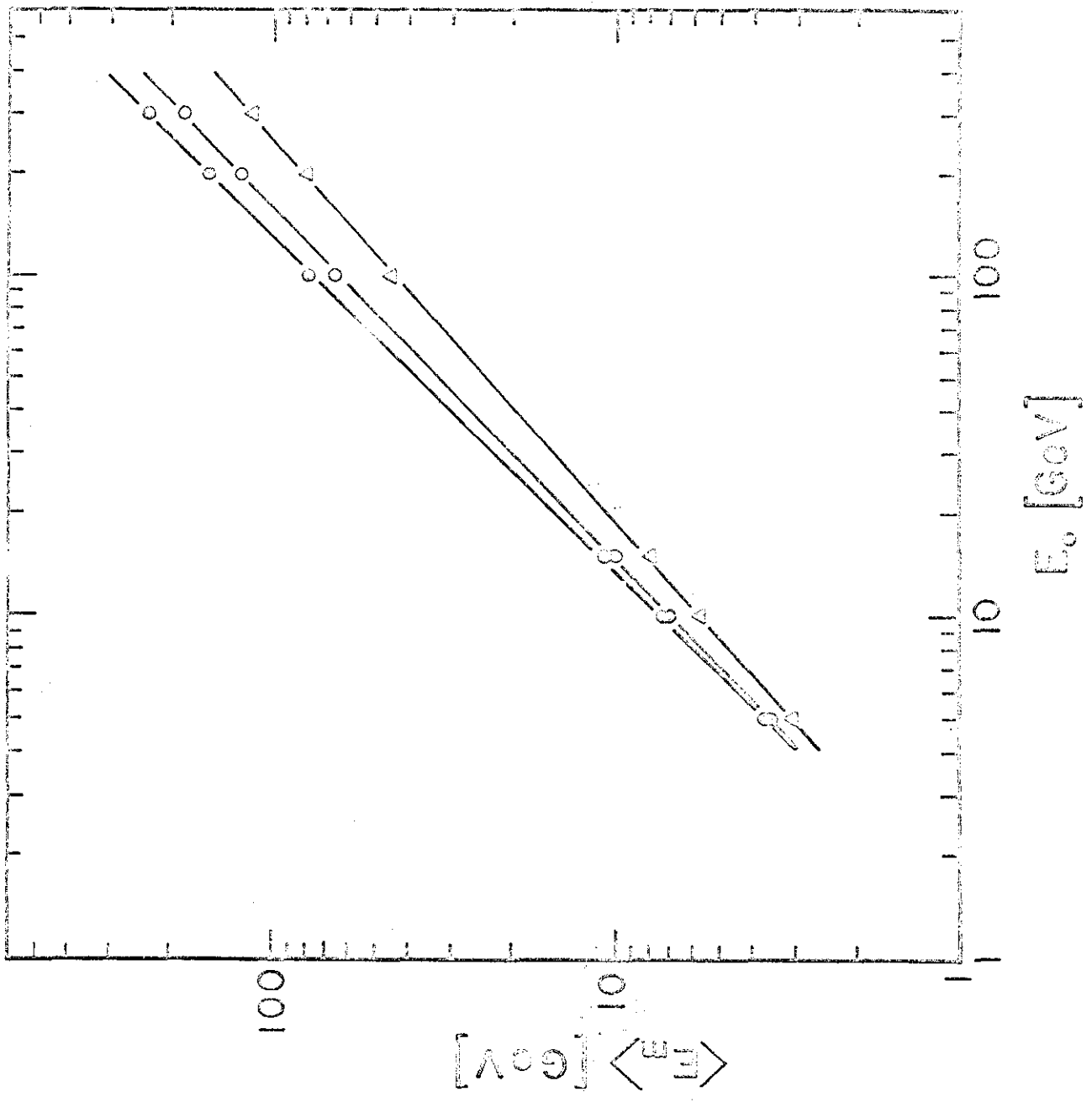


Fig. 5

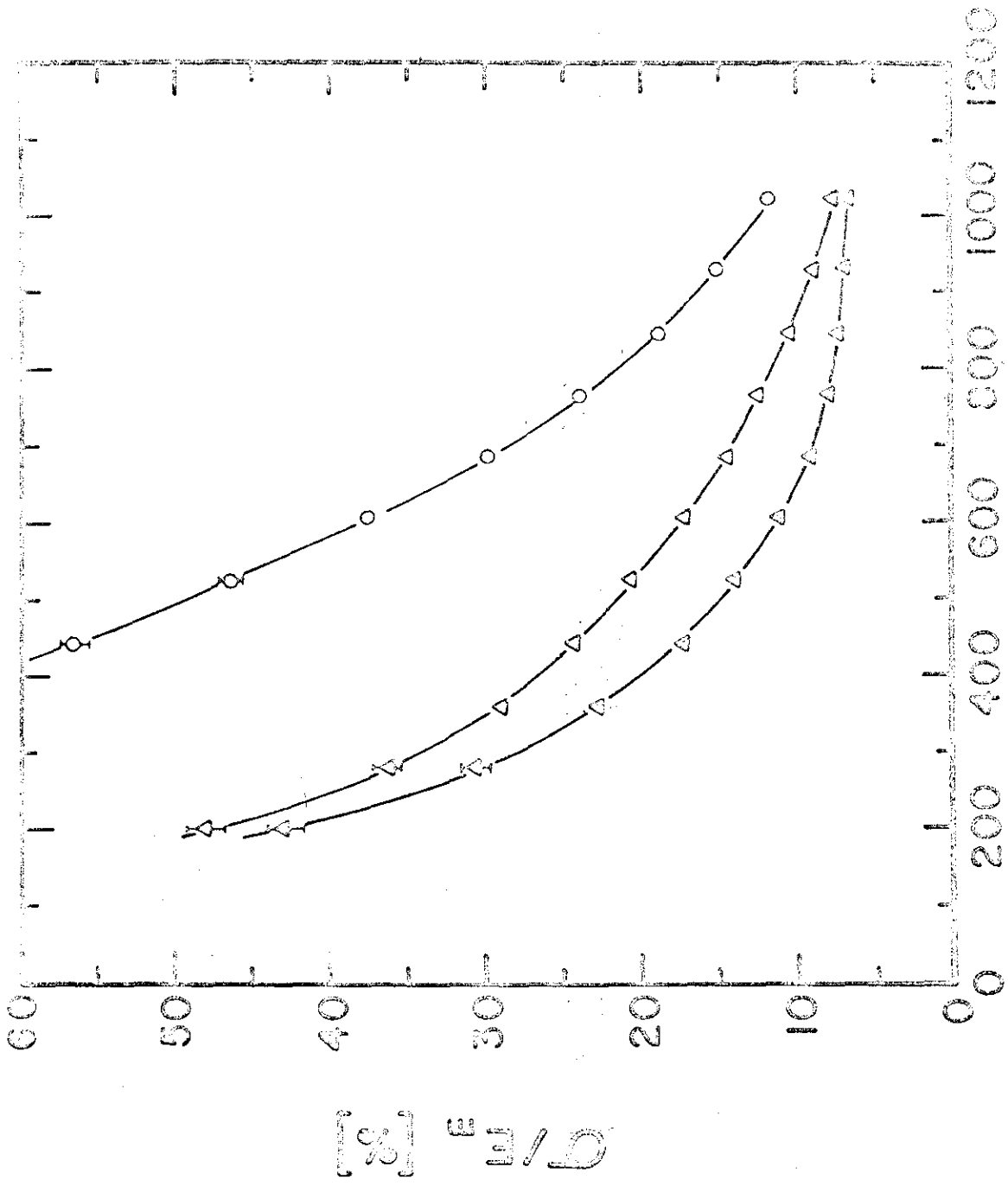
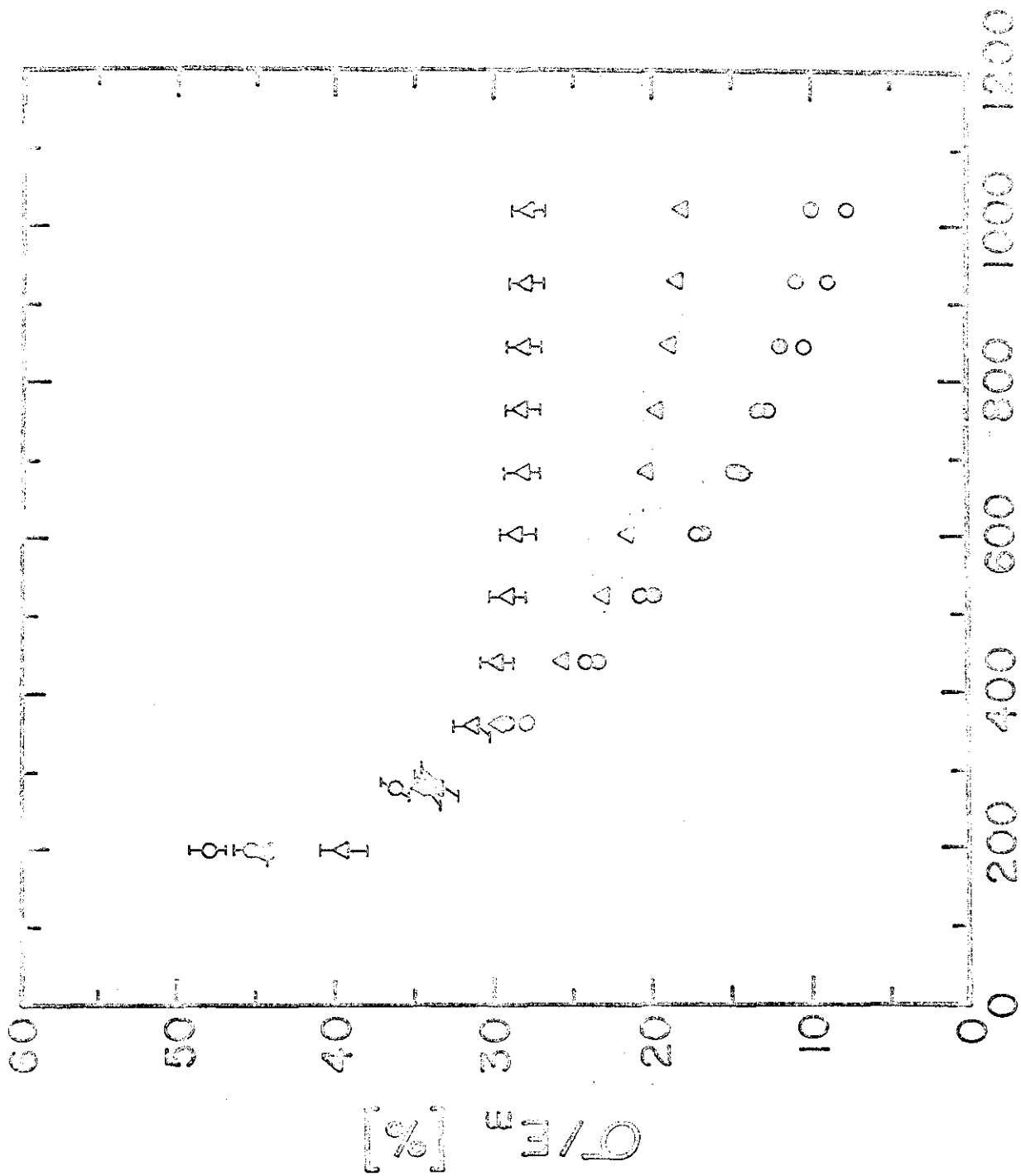


Fig. 6

1



t [g/cm²]

Fig. 7

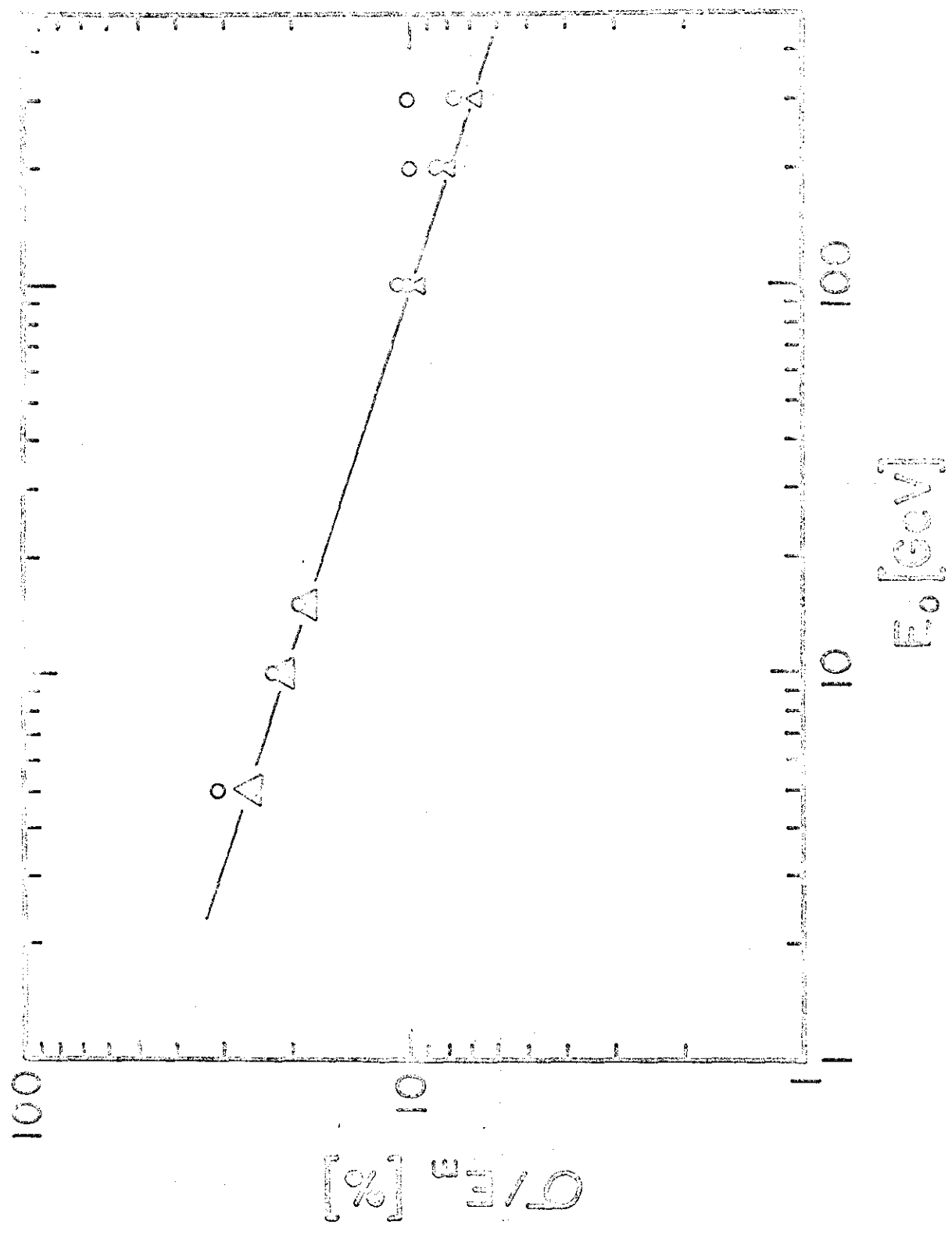


Fig. 8

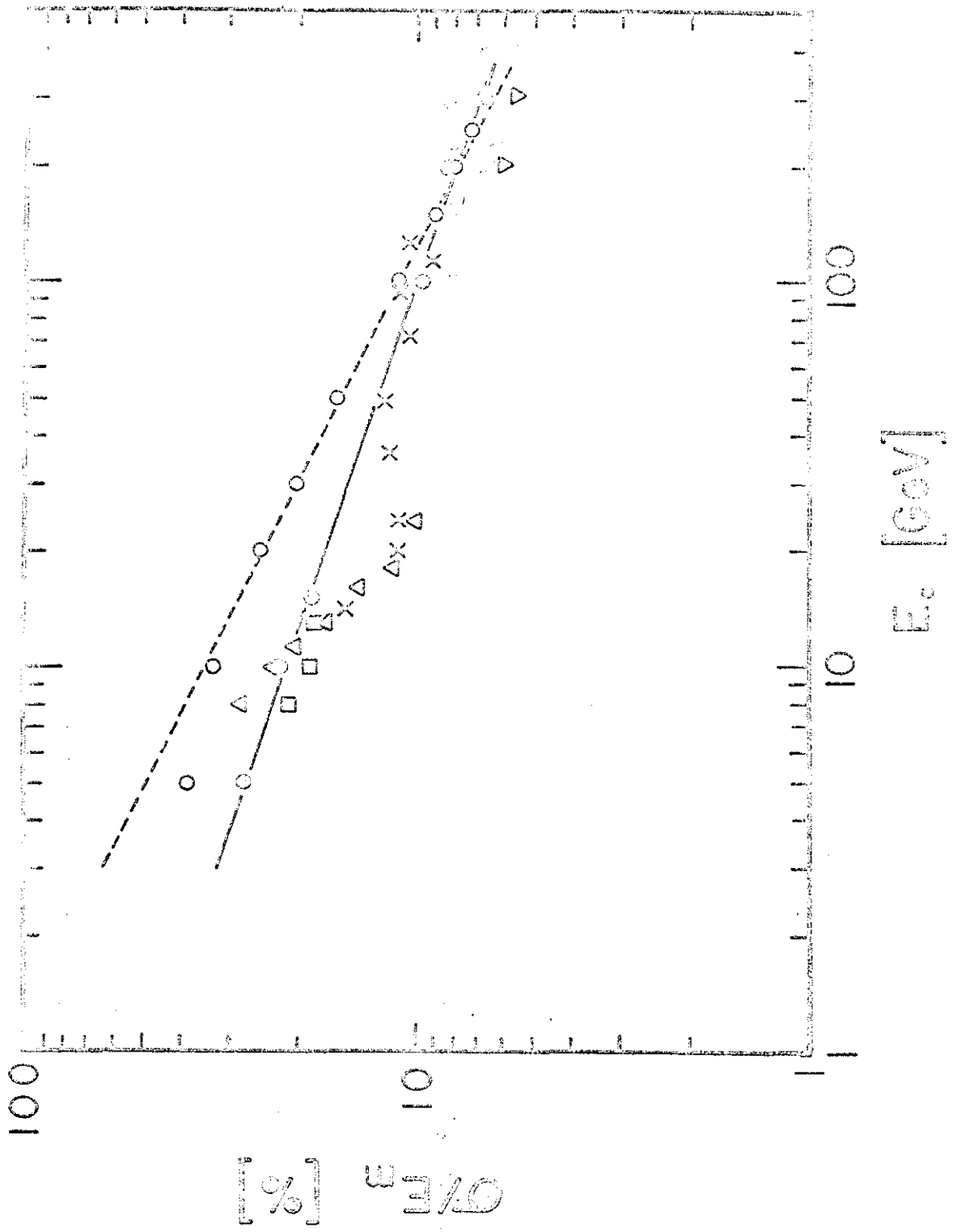


Fig. 9

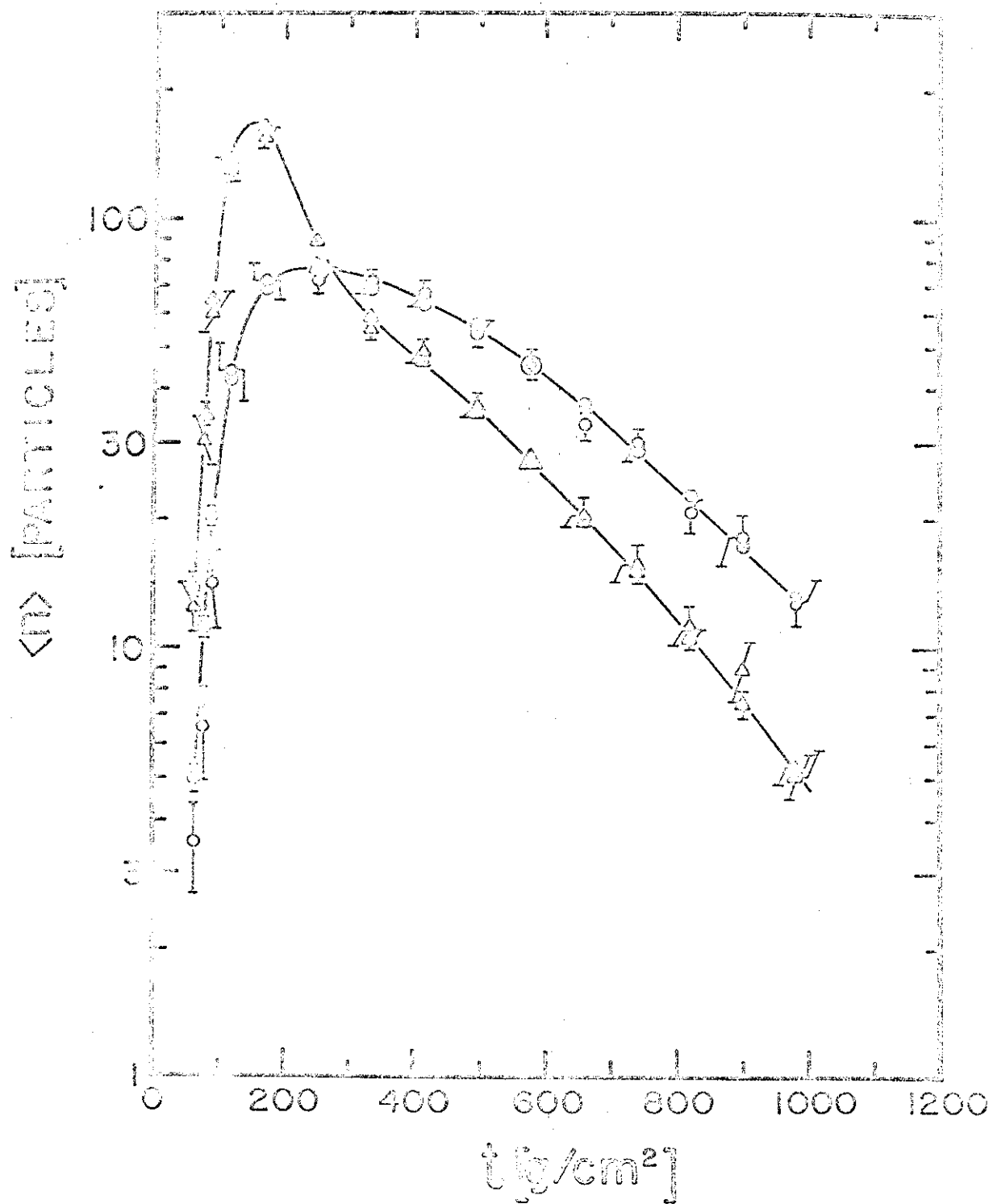


Fig. 10

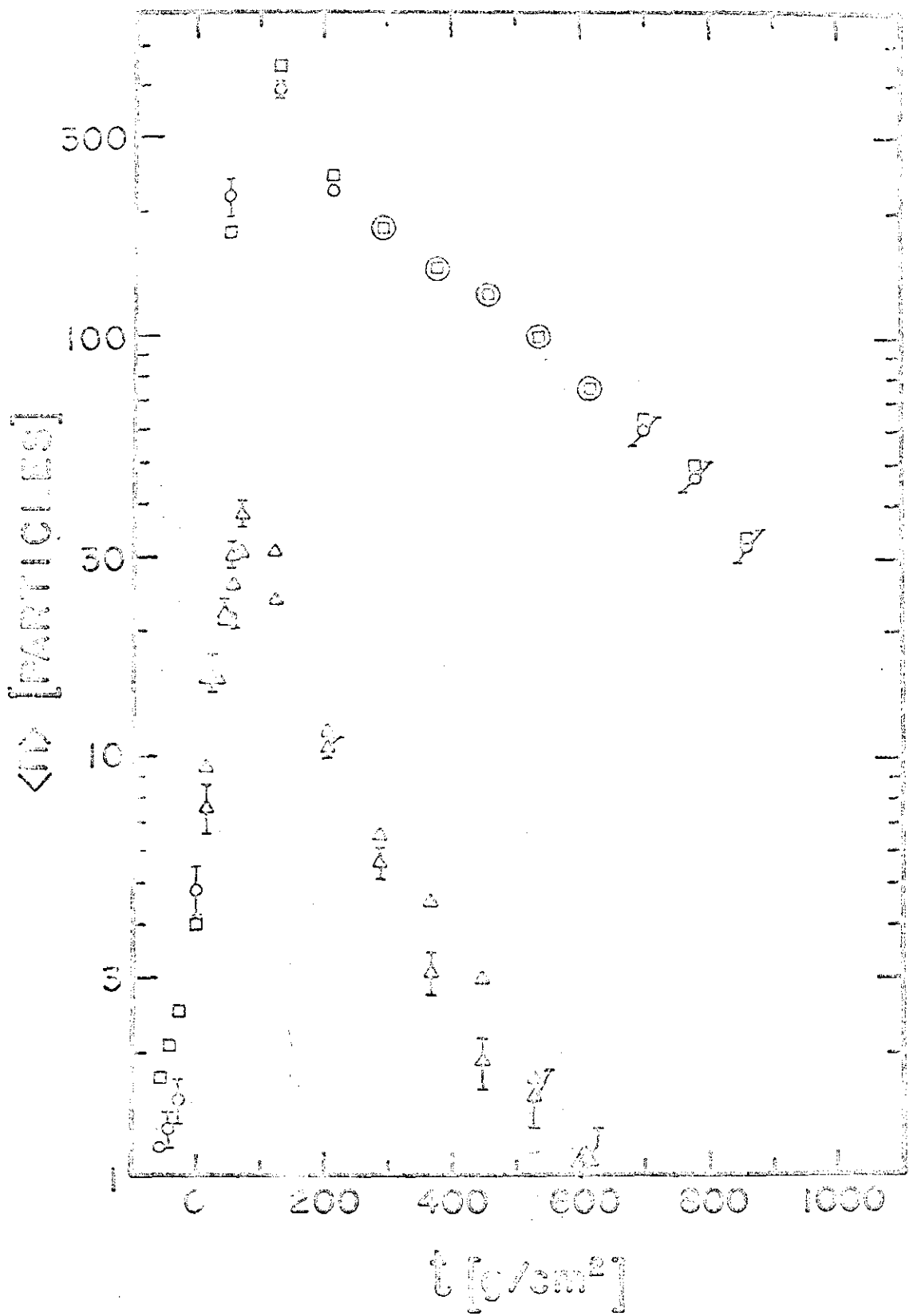


Fig. 11

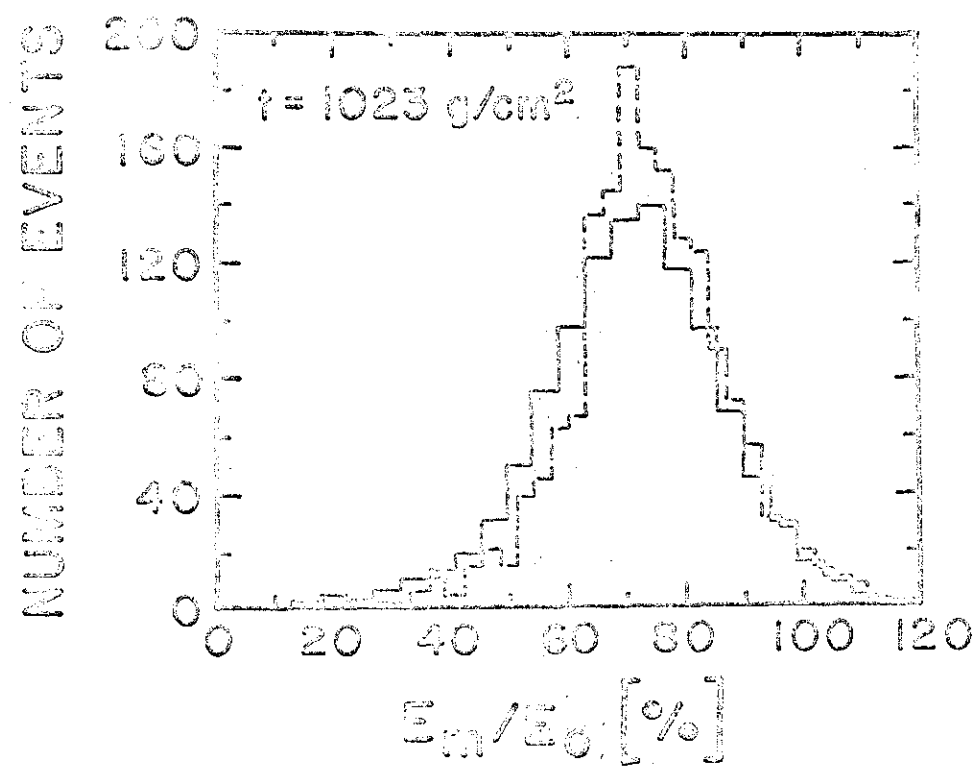
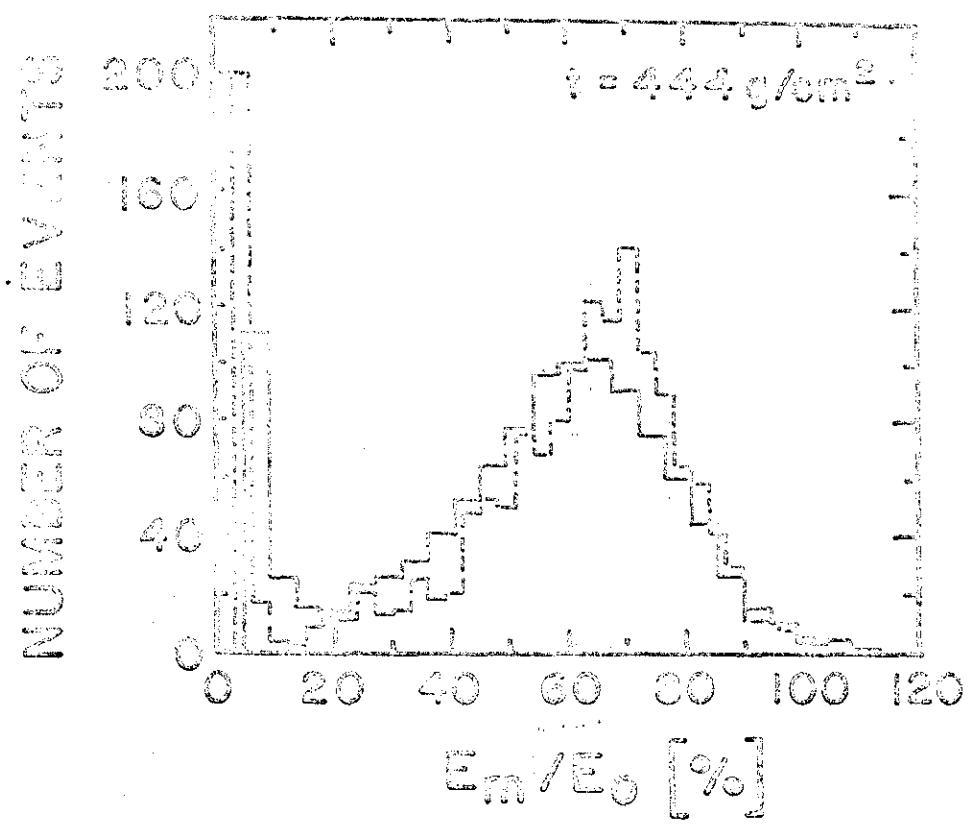


Fig. 12